Demonstration of an Axial PET concept for brain and small animal imaging

P. Beltrame[a], E. Bolle[g], A. Braem[a], C. Casella[b], E. Chesi[e], N. Clinthorne[f], R. De Leo[d], G. Dissertori[b], L. Djambazov[b], V. Fanti[a,1], C. Joram[a], H. Kagan[e], W. Lustermann[b], F. Meddi[h], E. Nappi[d], F. Nessi-Tedaldi[b], J. F. Oliver[c], F. Pauss[b], M. Rafecas[c], D. Renker[b,2], A. Rudge[e], D. Schinzel[b], T. Schneider[a], J. Séguinot[a], P. Solevi[c], S. Stapnes[g], P. Weilhammer[e]

[a]*CERN, PH Department, CH-1211 Geneva, Switzerland*
[b]*Institute for Particle Physics, ETH Zurich, CH-8093 Zurich, Switzerland*
[c]*IFIC, E-46071 Valencia, Spain*
[d]*INFN, Sezione di Bari, I-70122 Bari, Italy*
[e]*Ohio State University, Columbus, Ohio 43210, USA*
[f]*University of Michigan, Ann Arbor, MI 48109, USA*
[g]*University of Oslo, NO-0317 Oslo, Norway*
[h]*University of Rome "La Sapienza", I-00185 Rome, Italy*

Abstract

Standard Positron Emission Tomography (PET) cameras need to reach a compromise between spatial resolution and sensitivity. To overcome this limitation we developed a novel concept of PET. Our AX-PET demonstrator is made of LYSO crystals aligned along the z coordinate (patient's axis) and WLS strips orthogonally placed with respect to the crystals. This concept offers full 3D localization of the photon interaction inside the camera. Thus the spatial resolution and the sensitivity can be simultaneously improved and the reconstruction of Compton interactions inside the detector is also possible. Moreover, by means of G-APDs for reading out the photons, both from LYSO and WLS, the detector is insensitive to magnetic fields and it is then suitable to be used in a combined PET/MRI apparatus. A complete Monte Carlo simulation and dedicated reconstruction software have been developed. The two final modules, each composed of 48 crystals and 156 WLS strips, have been built and fully characterized in a dedicated test set-up. The results, obtained with a ^{22}Na point source (0.25 mm diameter), of the single module performances and a first estimation of the performances with the two module system are reported.

Key words: Positron Emission Tomography, Geiger-mode Avalanche Photo Diodes (G-APD)

1. Introduction

For a Positron Emission Tomography (PET) camera two parameters are relevant: (i) a good *spatial resolution*, which is fundamental to permit precise localization of tiny structures for brain mapping and for tumor contour, and (ii) the *detection efficiency*, which must be kept as high as possible in order to require low dose injection into the patient's body (or to enhance the image quality at the same dose level). Poor spatial resolution and low efficiency limit the performances of the clinical scanners. In standard cameras these limitations are mainly caused by the radial arrangement of the crystals with respect to the patient's axis: the poor (or absent) knowledge of the *Depth Of Interaction* (DOI) of the photon inside the crystal spoils the spatial resolution making it non-uniform in the whole *Field Of View* (FOV) because of the parallax errors, which increase with the crystal length. Reducing the length of the crystals could improve the resolution but, as drawback, reduces the detection efficiency. Moreover, the incapability of recognizing Compton interactions in the common PET cameras further degrades the image quality.

Taking into account these challenges, together with the diagnostic needs – which push towards multi-modalities exams, e.g. PET/MRI – has led our collaboration [1] to propose a completely different approach.

2. The Axial PET concept

The basic idea of the *Axial PET* (AX-PET) consists in the axial arrangement, along the axis of the scanner (z axis), of scintillating crystal layers interleaved by layers of *Wave Length Shifter* (WLS) strips, perpendicularly placed to the crystals.

When a 511 keV photon interacts inside one crystal, the light emitted within the total reflection cone travels through the crystal until reaching the photo detector. The light escaping from the crystal side where the WLS are placed is absorbed and re-emitted at different wavelength; then by internal reflection, as for the crystal, it is transmitted and read out. See Fig. 1 for a visual explanation of the process. Both the crystals and the WLS strips are individually read out by *Geiger-mode Avalanche Photo Diodes* (G-APD).[3] The DOI information (x coordinate in Fig. 1) is given by the knowledge of the

[1] On leave of absence from Università e Sezione INFN di Cagliari, Italy
[2] Currently with Technical University München, 85748 Garching, Germany
[3] Also known as SiPM and MPPC

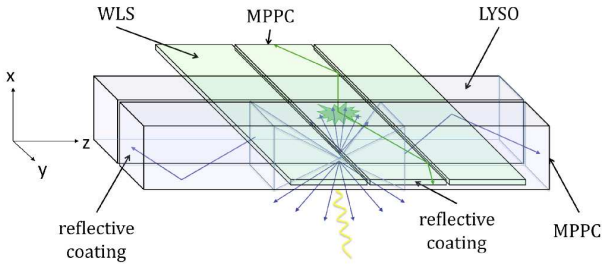

Figure 1: Two scintillating crystals (LYSO) placed parallel to the scanner axis z, and three WLS strips orthogonally placed to the crystals, show the Axial-PET concept. One side of the LYSO and of the WLS is equipped with G-APD (MPPC) while the other side has a reflective coating. The light emitted by the crystal is in part detected by the MPPC (either coming directly from the point of the scintillation or after having been reflected by the coating on the opposite side) and in part absorbed by the WLSs, whose signals permit to reconstruct the z coordinate.

layer of the hit crystal. So the crystal provides the radial position of the interaction (x and y coordinates) and the energy. The axial position (z coordinate) can be determined from the signal in the WLS strips.[4]

3. The Axial-PET demonstrator

The components. As scintillating crystals we use *LYSO*[5] bars from Saint-Gobain (PreLudeTM 420) of dimensions of $(3 \times 3 \times 100)$ mm^3. The LYSO is non-hygroscopic with a light yield of 32 photons/keV, attenuation length (at 511 keV) of 1.2 cm, scintillation decay time of 42 ns, single exponential. The WLS strips, from Eljen Technology (type EJ-280 with a dye concentration ten times higher than standard material), have dimensions of $(0.9 \times 3 \times 40)$ mm^3. They efficiently absorb the 425 nm light from LYSO and re-emit it at 490 nm. Both the LYSO and the WLS are readout by a G-APD, Hamamatsu *Multi Pixel Photon Counter* (MPPC). For reasons of compactness, the crystals and the strips are optically glued to their photo detector only on one side, while the other side is covered with an Al coating to make it reflective. The MPPCs used for the crystals are of standard type (S10362-33-050C, 3600 cells (50×50) μm^2, dimension (3×3) mm^2), for the strips they are custom made by Hamamatsu (OCTAGON-SMD, 782 cells (70×70) μm^2, dimension (3.22×1.19) mm^2). The MPPCs have been individually characterized in a dedicated set-up [4].[6]

Read out electronics. The signals out of the MPPCs are transmitted to fast amplifiers (OPA846). The output of each amplifier is threefold: (i) a direct short connection, via a 100 kΩ resistor turning the voltage signal into a high impedance current signal, to the *VATAGP5* chip [5]; (ii) in parallel the signals from the LYSOs are added together to build a pulse height sum which is used in the trigger; (iii) the signals of each channel are also available for test purposes.

The VATAGP5 chip has a fast and a "slow" branch. In the *sparse readout* mode of the chip only channels with a signal above a chosen threshold in the fast branch will be stored into the readout register, and the corresponding slow shaper amplitude of only these channels will eventually be read out.

The data acquisition works using the *external trigger*, which selects only events whose energy sum in the module (or in both the modules, see Sect. 5) is equal to 511 keV. The *self-triggering* feature of the readout is used for specific tests and for the energy calibration (see Sect. 4.1).

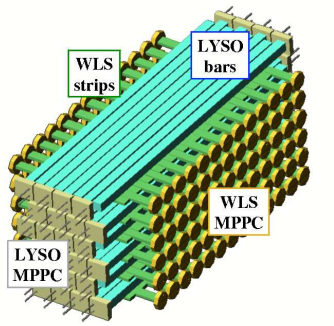

Figure 2: Drawing of one AX-PET module. Six layers of 8 crystals each are interleaved with six layers of WLS. The MPPCs are mounted alternately on one side of the module in order to avoid dead areas. The crystals in adjacent layers are staggered by half a pitch size.

The module. The AX-PET demonstrator is composed of two identical modules. Each module has 48 crystals and 156 WLS strips arranged in a stack of six layers, each layer with 8 LYSO bars and 26 WLSs, see Fig. 2. The pitch of the crystal plane is 3.5 mm, and 3.2 mm for the WLS plane. The distance between two layers, in the direction of the impinging photons, is 7 mm and each layer is optically separated from the next one by a thin carbon fiber plate. The crystals in even layers are staggered with respect to the crystals in odd layers by half the pitch size, so that the gaps between the crystals do not line up.

4. Single module characterization

The two modules were individually calibrated in a test set-up, using a point-like ^{22}Na source (activity of 925 kBq, diameter of 250 μm). Two tagging LYSO crystals of different dimensions, readout by a fast PMT, were used for the energy calibration and for axial spatial resolution studies. The different tagging crystals allowed to have either a uniform illumination of the module or a beam spot of about 1 mm on the module layer closest to the source. Both the taggers and the source holder were mounted on a computer controlled translation table for precise positioning of the source image on the module in two directions (y and z).

[4] The 511 keV photon from the photo absorptions in the crystals is easily observable in the WLS, while for Compton effects the photon must have an energy of at least 100 keV. Less energetic photons can be seen in the crystals but without the precise axial coordinate reconstruction [2, 3].

[5] The LYSO chemical formula is Lu1.8Y.2SiO5:Ce.

[6] Since the G-APDs are highly temperature dependent, this parameter is constantly monitored. The knowledge of the temperature permits to change the supply voltage of each photo detector in order to maintain a constant gain, or to apply an offline correction.

4.1. Energy calibration and resolution

To perform the energy calibration we used (i) data acquired in self-triggering mode, which comprise two of the peak positions of the ^{176}Lu decay spectrum at 202 and 307 keV, and the Lutetium K_α escape line at 63 keV, and (ii) data acquired with the ^{22}Na source and the larger tagging crystal, covering the photoelectric peak at 511 keV. The positions of the four peaks in the ADC versus Energy plot (see Fig. 3 as an example of one crystal) are fitted with a negative logarithmic function, $E(ADC) = p_0 - p_1 \cdot \ln(1 - \frac{ADC}{p_2})$. The about 5% saturation effect of the MPPCs occurring at the photoelectric peak energy, due to the finite number of cells capable to read out the photons from the crystal, is taken into account. All the 48 crystals of each module are calibrated by means of this "self calibration" technique.

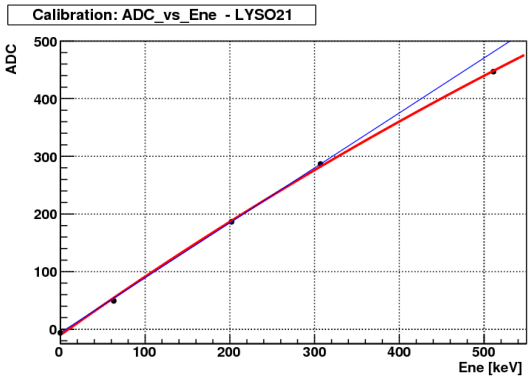

Figure 3: ADC vs. Energy plot showing the mean values of the Gaussian fits to the ADC distributions of the Lu intrinsic radioactivity, of the K_α escape line, and of the photo peak. The thicker line is the inverse of the negative logarithmic function used to fit the data. The deviation from the linear fit (straight line) is due to the MPPC saturation.

After the calibration, the average of the energy resolution of the LYSO crystals is $\Delta E/E$ = 11.6% FWHM (at 511 keV). Alternatively, as shown in Fig. 4, using the event by event energy sum in one module the resolution results to be 12.25% FWHM.

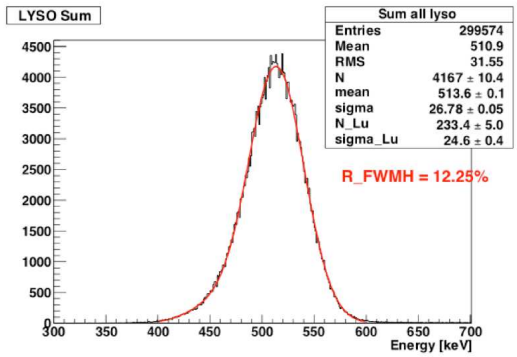

Figure 4: Energy distribution of the sum of all the crystals of one module. The relative width of this distribution is $\Delta E/E$ = 12.25% FWHM at 511 keV.

4.2. Spatial resolution

To estimate the resolution in the axial coordinate we collected data with the smaller tagger, to have a collimated spot size. Only photoelectric events, with one hit in the LYSO, are selected. The z position of the interaction inside the crystal is determined by means of a center of gravity of the WLS cluster. The measured spatial resolution, σ_{meas}, includes the intrinsic resolution σ_{intr} and the contribution of the beam spot size σ_{spot}, which increases with the distance d from the source:[7] $\sigma_{meas} = \sqrt{\sigma^2_{intr} + \sigma^2_{spot}}$. In order to extract the value of the intrinsic spatial resolution, σ^2_{meas} is extrapolated down to $d^2 = 0$, see Fig. 5. The result for σ_{intr} is 0.76 mm.

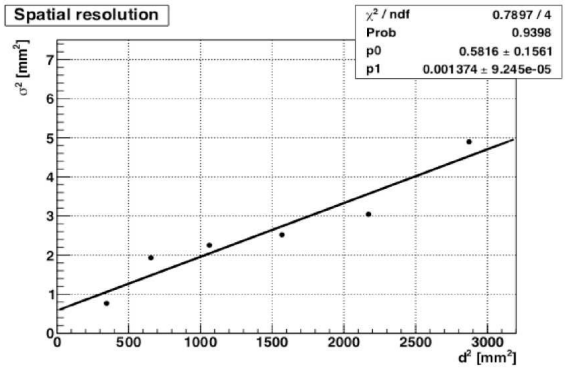

Figure 5: The six points represent σ^2_{meas} for each of the six layers as a function of the square of the distance of the layer from the source. The extrapolation to zero distance (p0) gives σ^2_{intr}.

5. Measurements with the two module in coincidence

The two modules were mounted in front of each other at 15 cm distance with the ^{22}Na source in the middle, see Fig. 6. Data were collected with the external trigger, see Sect. 3, requiring the energy sum to be equal to 511 keV in each of the two modules in coincidence.

Figure 6: Set-up for the two module coincidence data taking.

[7] The diameter of the spot is supposed to vary linearly with the distance d from the source.

5.1. Spatial resolution

To estimate the axial spatial resolution in the two module set-up we select photo peak events in both of the modules. Extrapolating the intersection on the central plane of the geometrical *Lines Of Response* (LOR), see Fig. 7 left, a resolution of 1.5 mm at FWHM is found, see Fig. 7 right. It is worth noting that the source size and the finite positron range are still included.

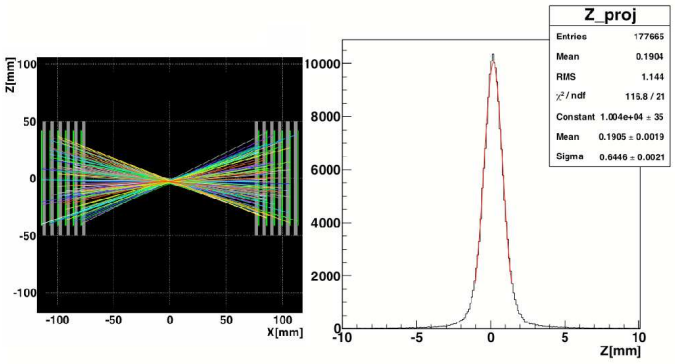

Figure 7: Left: side view of the two modules with the geometrical LOR selecting only photo peak events in both of the modules. Right: spread of the geometrical intersection of the LOR in the central plane between the two modules, providing an evaluation of the spatial resolution of the axial coordinate.

6. Simulation and image reconstruction

For a complete performance estimate of the entire system, the AX-PET demonstrator is fully simulated using `GEANT4` and `GATE` Monte Carlo packages. The former is used to model the optical transport and the geometry while the latter is a PET dedicated software capable of simulating time dependent phenomena, scanner rotation and source/phantom. In Fig. 8 the energy spectrum of the crystals is shown, demonstrating the excellent data-Monte Carlo agreement.

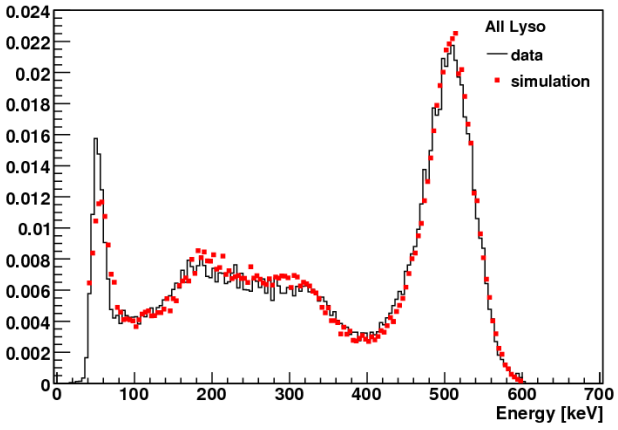

Figure 8: Comparison between data and Monte Carlo in the LYSO energy spectrum. The histograms have been normalized to one.

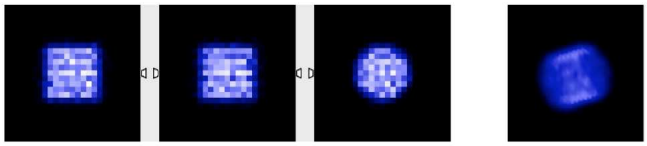

Figure 9: Reconstruction of a uniform cylinder source simulated in realistic run conditions. From the left to the right: x, y and z projection and 3D image.

The *image reconstruction software* is based on the *Maximum-Likelihood Expectation Maximization* (MLEM) algorithm [6]. The geometrical components of the System Matrix have been computed using Siddon's ray-tracing technique [7], in addition crystal attenuation and penetration effects have been taken into account. The code has been tested with several Monte Carlo phantoms. As an example in Fig. 9 the reconstruction of a simulated cylindrical source of 10 mm diameter and 10 mm hight is presented. A FOV of $(25 \times 25 \times 25)\,\mathrm{mm}^3$ in cubic Voxels of $1\,\mathrm{mm}^3$ each and six steps have been considered.

7. Conclusions and future plans

The AX-PET camera provides a three dimensional, parallax-error free localization of the photon interaction, the possibility of optimizing spatial resolution and sensitivity independently from each other, and the capability of recognizing Compton interactions inside the detector. Then, the Compton events can be either discarded to fully maintain the resolution, or they can be reconstructed, increasing in this way the sensitivity. The concept and all its components are MRI compatible and could be extended to perform Time-Of-Flight PET.

Two modules of the AX-PET demonstrator have been built and characterized. Preliminary results are very encouraging. An energy resolution of 11.6% FWHM at 511 keV as average of the single crystals is obtained. The spatial resolution in the axial direction is found to be 1.8 mm FWHM for photoelectric events, using a collimated beam spot. From the geometrical LOR intersections with the two modules in coincidence, the z-spatial resolution is 1.5 mm at FWHM.

The two modules will be mounted on a horizontal gantry, where the source and one of the modules can be rotated. In Spring 2010, at the ETH Zurich, first tomographic reconstructions of small animal phantoms will be performed, followed by the optimization of the Monte Carlo and reconstruction codes. In about one year, by means of further studies and simulations, possible specific geometrical options for a full scanner will be evaluated.

References

[1] `https://cern.ch/twiki/bin/view/AXIALPET`

[2] J. Séguinot et al., "Novel Geometrical Concept of a High Performance Brain PET Scanner- Principle, Design and Performance", Il Nuovo Cimento C, Volume 29 Issue 04 (2005) p 429.

[3] A. Braem et al., "Wave Length Shifter Strips and G-APD Arrays for the Read-Out of the z-Coordinate in Axial PET Modules", Nucl. Instr. and Meth. A 586 (2008) 300-308.

[4] E. Bolle at al., “Development of a High Precision Axial 3-D PET for Brain Imaging”, Nuclear Physics B (Proc. Suppl.) 197 (2009) 19-23.
[5] E. Chesi at al., “A segmented hybrid photon detector with integrated auto-triggering front-end electronics for a PET scanner”, Nucl. Instr. and Meth. A 564 (2006) 352-363.
[6] L.A. Shepp, Y. Vardi, ”Maximum likelihood reconstruction for emission tomography”, IEEE Trans. on Medical Imgaging, Vol. 1 (1982) 113-122.
[7] R.L. Siddon, ”Fast calculation of the exact radiological path for a three-dimensional CT array”, Medical Physics, Vol. 12, 02 (1985) 252-255.